Environ Earth Sci (2016) 75:1342
DOI 10.1007/s12665-016-6107-2

ORIGINAL ARTICLE

The application of inverse modeling in characterizing hydraulic conductivity beneath the city of Berlin, Germany

Alireza Hassanzadegan[1] · Mauro Cacace[1] · Judith Sippel[1] · Magdalena Scheck-Wenderoth[1]

Received: 18 January 2016 / Accepted: 20 September 2016 / Published online: 12 October 2016

Abstract In geothermal reservoir characterization and basin modeling, often conclusions are drawn and decisions are made using uncertain or incomplete data sets. Particularly, there are limited hydrogeological data in the Berlin area in the North German Basin. The groundwater in this sedimentary basin is divided into a shallow freshwater aquifer (with about 500 m depth) and a brackish to saline groundwater aquifer within deeper sedimentary layers. Between these two different groundwater compartments, a natural hydrogeological boundary is provided by the presence of an impervious clay-enriched layer (Rupelian Clay), which is discontinuous, eroded or not deposited in some local areas. Thereby, the distribution of hydraulic conductivity of Rupelian Clay aquitard that represents a vertical and horizontal partitioning of the aquifers below Berlin is of main importance in groundwater management. We use an inverse modeling approach to estimate the spatial distribution of hydraulic conductivity of the Rupelian Clay aquitard, using available local data within the Berlin province. We use a commercial finite element fluid flow simulator that interfaces to a parameter estimation package. A Gauss–Levenberg–Marquardt algorithm is used to adjust the hydraulic conductivity of the aquitard such that the hydraulic head observations are reproduced. Subsequently, the updated hydraulic conductivity of the Rupelian Clay is used as input to the forward modeling, in order to estimate the pressure and temperature fields. The results of the inverse modeling suggest a more continuous distribution of the Rupelian Clay layer below the Berlin area in comparison with previous published studies. Hence, the convective heat and fluid flow are more restricted, and there is less interaction between shallow and deep aquifers. Change in the predicted temperature field is more pronounced for deeper strata.

Keywords Hydraulic conductivity · Inverse modeling · Parameter estimation · North German Basin

✉ Alireza Hassanzadegan
alireza.hassanzadegan@gfz-potsdam.de

[1] Helmholtz-Zentrum Potsdam GFZ German Research Centre for Geosciences, Potsdam, Germany

List of symbols

Greek letters

β	Vector of unknown parameters
ϵ	Porosity
Λ	Thermal heat conductivity
μ	Viscosity
ω	Multiplier
Φ	Objective function, sum of squares of residuals
ψ	Pressure head values
ρ	Density

Roman letters

$\hat{g}$	Acceleration unit vector
b	Upgrade vector
c	Heat capacity
e	Residual vector
g	Gravitational acceleration
H	Hessian matrix
e	Residual vector
g	Gravitational acceleration
H	Hessian matrix
h	Hydraulic head
I	Unit tensor
J	Jacobian matrix

K Conductivity
P Groundwater recharge or infiltration rate
p Pressure
Q Source/sink term
q Darcy fluid flux
S Saturation, storage
T Temperature
t Time
X Matrix of known measurements
y Observation vector

Subscripts
0 Initial
j Coordinate number
m Measurement
p Parameter
r Regularization, residual
y Yield

Superscripts
e Element
f Fluid
s Solid
T Transpose matrix

Introduction

Accurate estimation of groundwater model parameters can be difficult, especially for very large aquifer systems and in the presence of limited data. In geothermal reservoir characterization and basin modeling, it is often required to draw conclusions and make decisions using uncertain or incomplete data sets. Among different hydrogeological properties, hydraulic conductivity is the most important parameter and one of the most difficult parameters to estimate. Not only the preferential flow path is controlled by high hydraulic conductivity units but also the thermal field is influenced by variations of hydraulic conductivity as a result of variations in advective heat transfer processes. Moreover, the knowledge of hydraulic conductivity of sedimentary units is essential to determine the hydraulic decoupling between shallow and deep aquifers (Godderniaux et al. 2013). The spatial distribution of hydraulic conductivity can be obtained either by direct laboratory and field measurements or by assimilation of available information using inverse modeling.

Inverse modeling helps the modeler to use available data and to estimate model input parameters by means of optimization techniques. The statistical and geostatistical approaches to estimate spatially varying aquifer transmissivities under steady-state and transient conditions are of fundamental importance. An statistical approach was developed by Neuman and Yakowitz (1979); Carrera and Neuman (1986) and applied to a real aquifer in Cortaro Basin Neuman et al. (1980). Kitanidis (1998) employed a geostatistical approach, i.e., the logarithms of transmissivity, random functions and variograms, to solve the inverse problems. A more computationally efficient scheme based on variational methods was introduced by Neuman (1980) that eliminated computing derivatives of hydraulic conductivity. Poeter and Hill (1997) discussed the requirements and benefits of the nonlinear least-square regression approach. Hill and Osterby (2003) presented the information that can be obtained from parameter correlation coefficients, particularly extremely correlated parameters, and compared them with the method of singular value decompositions (SVDs). A more recent field study is based on the 3D hydraulic tomography approach that provided a powerful method for reducing uncertainty in aquifer characterization. Thereby, several pumping and observation wells were employed, and flow rates and changes in hydraulic head were recorded at different locations (Cardiff et al. 2013). A comprehensive review that analyzed and tracked the evolution of inverse methods is given by Zhou et al. (2014).

A fairly complex vertical partitioning of aquifers and aquitards has been observed particularly in the hydrogeological system beneath the city of Berlin, as a part of the North German Basin (NGB). The subsurface beneath the city of Berlin is characterized by a system of regional aquifers of varying salinity content separated by the presence of regional aquitard formations. Among the latter, the Rupelian Clay is of special interest and concern since it hydraulically divides the shallow (Quaternary) freshwater aquifers on top from the deeper, brackish to saline Mesozoic aquifers beneath it (Magri et al. 2005, 2009). However, the Rupelian Clay is not a continuous layer, and both the top and the base of the Rupelian Clay are marked by some unconformities (Kaiser et al. 2011). It is missing in some areas within the basin, eroded or not deposited, which hereafter are referred to as hydrogeological windows (Kaiser et al. 2011). The current study focuses on the hydrogeological system and the subsurface below the city of Berlin, and in particular on the distribution of the Rupelian Clay aquitard.

As the spatial distribution of the Rupelian Clay controls the hydraulic partitioning between shallow and deep aquifers, it is the subject of study in different disciplines, such as water resource management, basin analysis and geothermal energy exploration. The fresh and salty water may interface and interact where the Rupelian Clay is missing and hence alter the salinity, pressure and temperature distributions, at both shallow and deep aquifers. How deep this effect is, is still an open question. Likewise, the primary questions in the application of geothermal

reservoirs are: where to drill, how to design and complete the well, and how is the initial distribution of temperature and pore pressure in the NGB? The answer to these questions requires that the spatial distribution of hydraulic conductivity as represented by the Rupelian Clay distribution, in concert with other properties, initial and boundary conditions, is properly known.

The position and extent of the hydrogeological windows are not precisely known (Limberg et al. 2014). If a one-to-one correlation between hydraulic conductivity and lithology of the Rupelian Clay can be assumed, inverse modeling can support the assessment of the spatial distribution of the Rupelian Clay by estimating hydraulic conductivity of this layer. This implies that areas where the deep and shallow aquifers are connected are distinguished by a vertically continuous fluid flow and hydrogeological window (high hydraulic conductivity), where the distribution of impervious Rupelian Clay is discontinuous. In order to characterize this unconformities, we apply an inverse modeling approach to a preexisting 3D geological model ("Initial model: hydrogeological system of Berlin" section). This is done in order to better constrain the distribution of the Rupelian Clay aquitard and thus the lateral variation in hydraulic conductivity, where there are no or limited field and laboratory measurements.

Accordingly, the goal of this study is to derive an improved distribution of the Rupelian Clay aquitard and to determine the interrelation between over and underlying (shallow and deep) aquifers. This study provides the application of inverse modeling for a large-scale 3D model. While the focus of many inverse modeling studies quoted above was on identification of hydraulic parameters within the aquifers, this study pays particular attention to geological structure of Rupelian Clay aquitard, i.e., the presence or absence of Clay layer. In the following, we first present the hydrogeological setup and available hydraulic head data related to the shallow freshwater aquifers (observation parameters). Then, we present our inverse modeling approach and the tools that we use to minimize the sum of the quadratic differences between observed and calculated hydraulic heads. Finally, we discuss and verify the results of our inverse modeling approach and present an improved prediction from an optimized forward simulation of coupled fluid and heat transport.

Initial model: hydrogeological system of Berlin

Berlin is located in the southeastern domain of the North German Basin (NGB). A preexisting model of the Berlin subsurface has been utilized here as initial model, knowing that the spatial distribution of the Rupelian Clay within this model includes a high degree of uncertainty. This 3D model integrates three main sources of information at different scales:

1. the sedimentary sequence derived from a 3D lithospheric model of Brandenburg with a horizontal resolution of 1 km,
2. The 3D hydrostratigraphic model of Cenozoic units in Berlin with a horizontal resolution of 0.5 km (Jaroch 2006) and
3. Stratigraphic and lithological data from four deep boreholes located in the area of Berlin or close to its political border.

The area covered by the model is 43.5 $\times$ 53 km in the horizontal extension and reaches down to 6 km below mean see level (see Fig. 1). From top to bottom, the 3D structural model consists of the following stratigraphical units: a Quaternary aquifer, 3 Tertiary units above the Rupelian Clay, a Pre-Rupelian Tertiary unit, Upper Cretaceous, Lower Cretaceous, Jurassic, Upper Triassic (Keuper), Middle Triassic (Muschelkalk), Lower Triassic (Upper, Middle and Lower Buntsandstein), Permian Zechstein, Permian Rotliegend, Permo-Carboniferous Volcanics and a pre-Permian basement (see Fig. 1).

Hydrogeological settings

Most of the surface area in Berlin is covered by Quaternary fluvial and glacial deposits. In general, Quaternary deposits are described as unconsolidated sands alternating with clays and silts, and glacial till of ground moraines related to the Pleistocene, starting some 2.6 million years ago (Stackebrandt 2010). The Tertiary sediments underneath the Quaternary strata consist of marine deposits, of which the Rupelian Clay aquitard forms the largest part. Figure 2 illustrates a thickness map of the Rupelian Clay with the geometry of hydrogeological windows as included in the initial geological model. The base of freshwater aquifer system of Berlin is widely formed by the top of the Rupelian Clay unit (Fig. 3). The Rupelian Clay is located at depths of -9 to 544 m below sea level, with an average burial depth of 152 m. This unit reaches the maximum burial depth of some 540 m in the Northwest of Berlin.

The Mesozoic units mainly consist of fine-grained clastic sediments (silt- and claystone) and carbonates. Only some formations contain a larger amount of sandstone and consequently posses a higher hydraulic conductivity. Among them, the Middle Buntsandstein is the thickest formation and provides favorable conditions for fluid flow. Two other semi-impervious stratigraphical units (in addition to an impervious basement) are the Middle Triassic Muschelkalk that consists of a sequence of limestone and dolomite beds with intercalated evaporates and clays, and the Zechstein unit consists predominantly of rock salt. Both

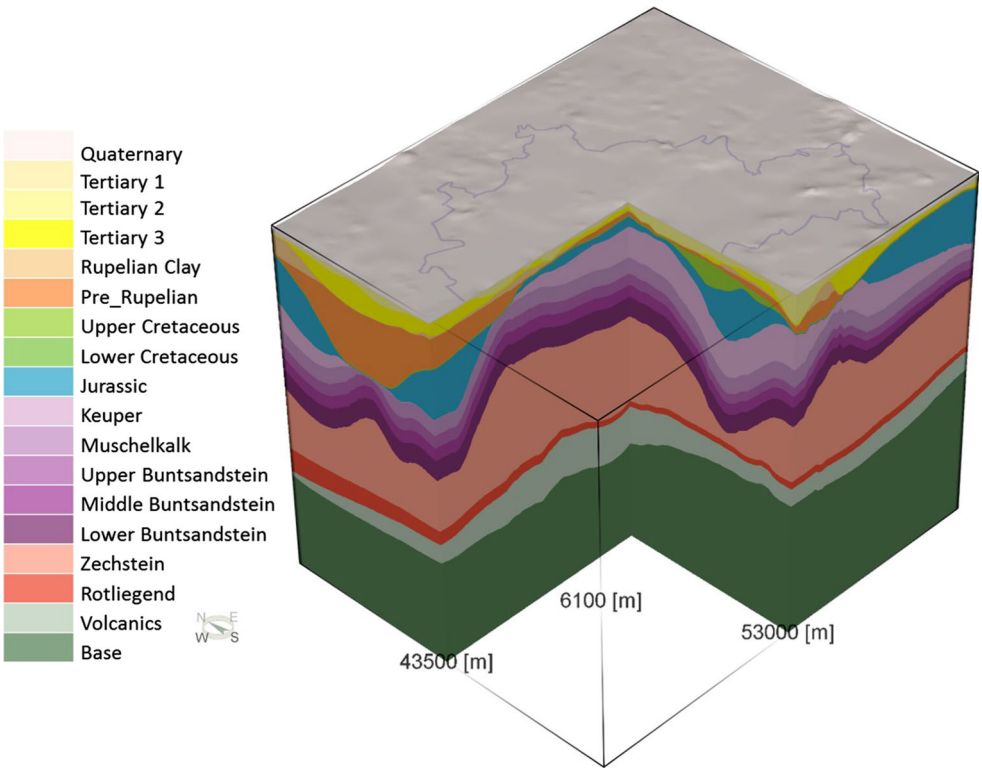

Fig. 1 3D structural model of Berlin. The Rupelian Clay is missing in some area, eroded or not deposited. The *solid line* on the surface presents the Berlin border

the Muschelkalk and the Zechstein Salt transmit water at a very low rate compared to the other sedimentary units. The Muschelkalk layer separates the Buntsandstein aquifers below, from the Keuper and Cretaceous aquifers above. Likewise, the Zechstein layer separates the sedimentary Rotliegend aquifer below, from the Buntsandstein aquifer above it. The Permo-Carboniferous volcanic rocks are mostly composed of rhyolites and andesites. Below the Permo-Carboniferous volcanics, the model basement consists of a layer of strongly compacted pre-Permian metasedimentary rocks.

Numerical model and parametrization

Based on this initial structural model, a 3D finite element mesh has been created to perform the numerical simulation of subsurface fluid flow and heat transfer. The numerical model consists of 55 simulation layers aligned with the geological structures, formed by the 18 distinct stratigraphical layers. The model domain is discretized by 4,057,680 prismatic triangular elements of the size 250 × 250 m, with a varying thickness between 2.5 to 875.5 m.

FEFLOW requires all layers to be continuous; thus, the initial model considered the hydrogeological windows within the Rupelian Clay layer by assignment of the same hydraulic conductivity of the over and underlying layers (Fig. 2b). The numerical model approximates all geological units as homogeneous layers, where the material properties are constant within each layer, apart from the Rupelian Clay layer. Consequently, the simulation model was populated with hydraulic and thermal properties as listed in "Appendix 1".

In order to ensure a correct representation of low flow velocities in the aquitard and to minimize errors due to the nodal nature of the velocity field, the Rupelian Clay aquitard was subdivided into three simulation layers, albeit the same hydraulic parameters and physical properties were assigned to them.

An initial hydraulic conductivity of 10^{-3} m day^{-1} was assigned to the hydrogeological windows within Rupelian Clay layer, and a lower hydraulic conductivity of 10^{-8} m day^{-1} was assigned to the Rupelian Clay units. The hydraulic conductivity of the sandstone units range between 6.7×10^{-4} and 6×10^{-2} m day^{-1} for different layers and formations.

Inverse modeling approach

In order to characterize the hydraulic conductivity distribution of the Rupelian Clay, a forward fluid flow simulator was combined with an inverse modeling technique for parameter estimation. Therefore, FEFLOW^{TM}, a finite element commercial software (Diersch 2014), and the parameter estimation program PEST (Doherty 2002) were employed.

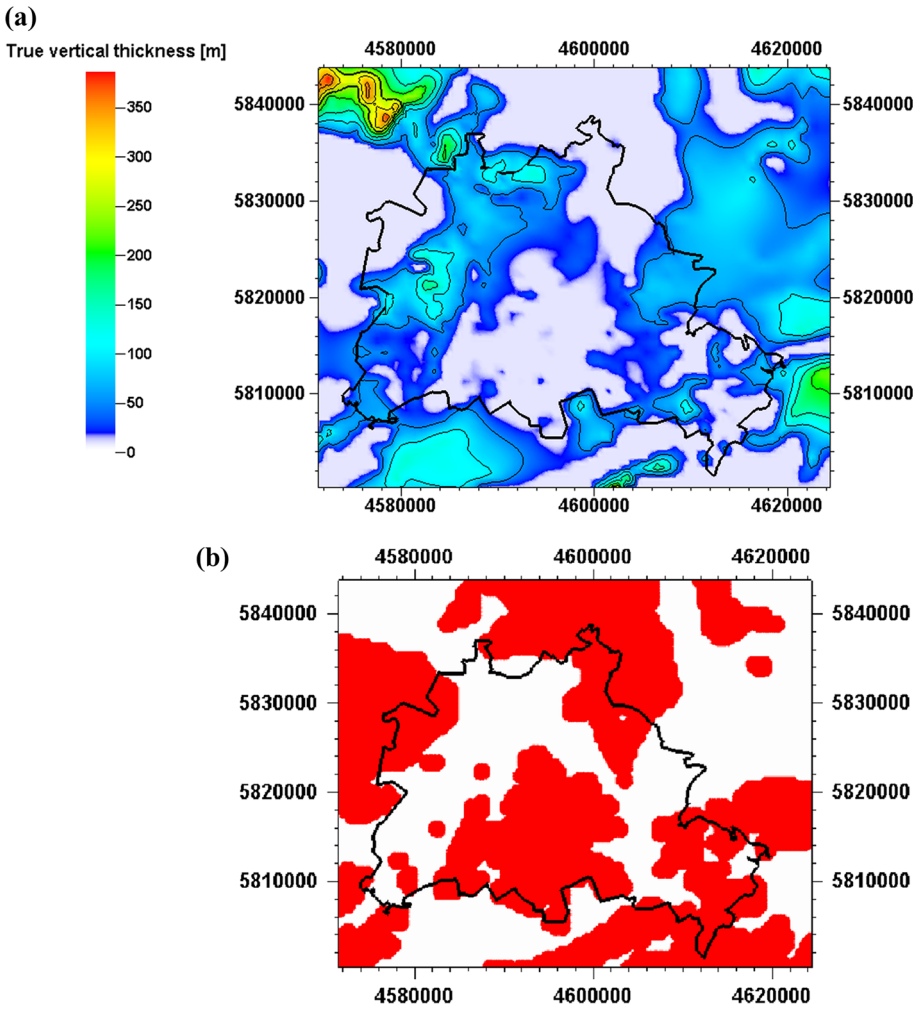

Fig. 2 Initial Rupelian Clay thickness and hydraulic conductivity maps. **a** Initial Rupelian Clay thickness map. In the initial model, hydrogeological windows are assumed to represent areas where the Rupelian Clay is missing (*light blue areas*). **b** The hydrogeological windows (in *red*) were defined as hydraulically conductive zones having similar hydraulic conductivity of 0.001 m day^{-1} as the upper and lower adjacent layers in the initial model. The initial hydraulic conductivity of the Rupelian Clay was as low as 10–8 m day^{-1}

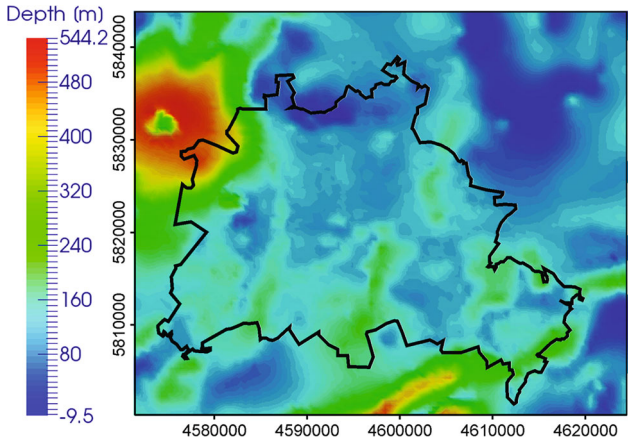

Fig. 3 Depth distribution of top Rupelian Clay (meter below sea level)

Figure 4 shows the coupled modeling workflow. FEFLOW runs an initial forward simulation where hydraulic conductivity K is an input parameter and hydraulic head h is the result of modeling (step a of Fig. 4). PEST reads the results (output file) of the FEFLOW simulation, which includes the calculated hydraulic heads, and compares them with measured hydraulic head values (steps b and c of Fig. 4). Subsequently, PEST uses an optimization technique in order to minimize the sum of the squared difference between observed and calculated hydraulic head values, e.g., by adjusting the hydraulic conductivity K (steps d, e and f of Fig. 4).

In order to minimize the squared difference between observed and calculated hydraulic head, PEST increases or decreases the value of the input hydraulic conductivity K^i (the superscript i refers to initial) and creates a new FEFLOW input file with the newly estimated hydraulic conductivity K^n (steps e, f, g and h of Fig. 4). Subsequently, FEFLOW calculates a new hydraulic head value h^n. For the new FEFLOW model, PEST compares the old and new files and calculates the sensitivity of the changing hydraulic head with respect to hydraulic conductivity, $\frac{(h^i - h^n)}{(K^i - K^n)}$. This iteration continues until the sum of the squared difference between calculated and measured hydraulic

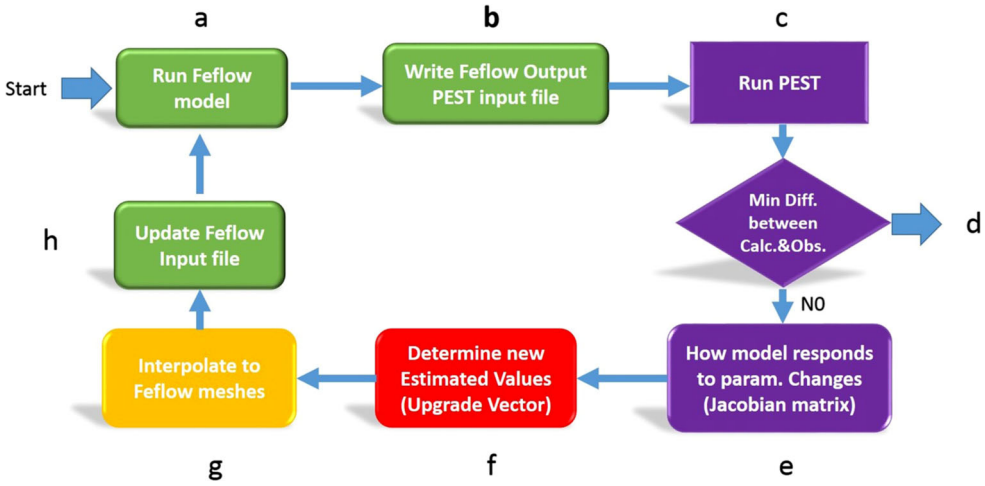

Fig. 4 The spatial distribution of hydraulic conductivity was determined by an iterative approach, whereas the difference between observed and calculated hydraulic head values was minimized

heads is minimized and arrives at the exit point (step *d* of Fig. 4).

Therefore, the first step in the inverse workflow is to solve for Darcy's law and to calculate *h* having an initial value for *K* by means of a FEFLOW forward simulation. The second step is to compare the calculated and measured *h* using an objective function (see "Appendix 3"). The third step is to evaluate the model fit and adjust the *K* values by utilizing an optimization technique provided by the parameter estimation package, PEST, to minimize the objective function (Doherty 2002).

FEFLOW: applied boundary conditions

FEFLOW is a finite element software that simulates coupled fluid flow and heat transport in variably saturated media. Therefore, the numerical simulation approximates the solution by considering the physical processes involved and solves for partial differential equations that are derived from Darcy's law, fluid mass conservation and energy conservation ("Appendix 2"). The main heat transport processes involved are heat conduction (thermal diffusion), due to temperature difference, natural convection, due to density differences, and advection (forced convection), due to hydraulic head differences (e.g., see "Appendix 2," Eq. 1).

Thermal boundary conditions

Thermal boundary conditions were applied to the earth surface and to the base surface (bottom slice) of the model at 6 km below sea level. The temperature at the surface was assumed to be constant at 10 °C, and a spatially varying temperature distribution was applied at the base surface of the model, as derived from a full lithosphere-scale, purely conductive thermal model.

Hydraulic boundary conditions

A common assumption for the hydraulic head boundary conditions is to have hydraulic head as equal to the topographic elevation. A more realistic approach is to consider the upper hydraulic boundary as a free (phreatic) surface. The shape of the free surface is initially assumed to be unknown, that is, geometrically the surface border is fixed, while its curvature is allowed to vary. By running the model in steady state, the hydraulic head distribution is calculated and the location of the free surface is determined (see "Appendix 2").

PEST: parameter estimation

PEST is using an iterative approach to determine the optimized set of parameters and create a new FEFLOW input file. The major steps are

a. to calculate the sensitivity of hydraulic head values with respect to hydraulic conductivity values, Jacobian matrix (*J*), and
b. to obtain a parameter upgrade vector *b* (see "Appendix 3").

The FEFLOW model introduced as initial model in "Initial model: hydrogeological system of Berlin" section was utilized, and the phreatic boundary condition was applied. The digital hydraulic head map consists of more than 17662 points (observation points). To decrease the execution time, the digital hydraulic head map was resampled using 31 data points. The resampled map assured an accuracy of ±1.5 m. These measured hydraulic head values (observations) were used to constrain and adjust the Rupelian Clay hydraulic conductivity that produced the best possible fit to the calculated hydraulic head values (Fig. 5). This set of hydraulic conductivity values for the Rupelian Clay layer was defined as calibrating parameters.

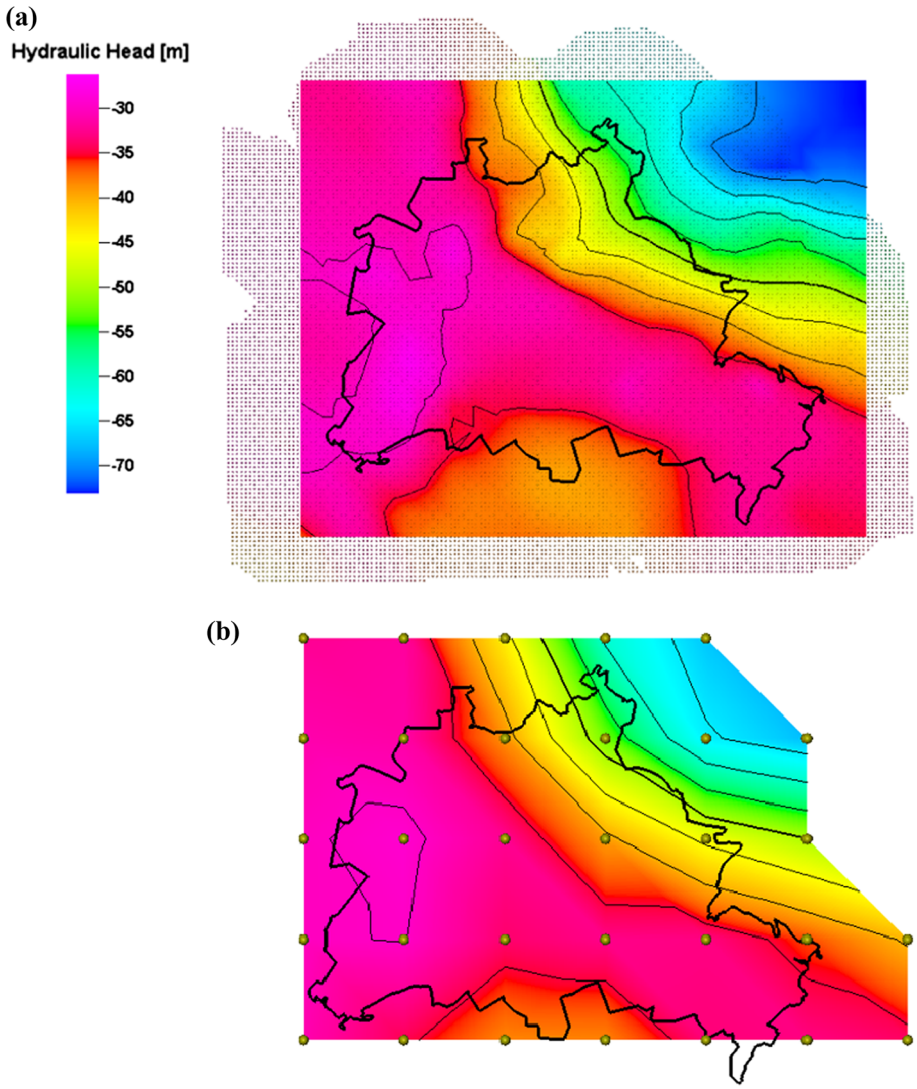

Fig. 5 Hydraulic head map and observation points. The polygon represents Berlin border. The observation points were used in PEST to adjust the hydraulic conductivity of the Rupelian Clay layer. **a** Initial hydraulic head map includes 17662 data points. **b** The hydraulic head map was resampled by 31 observation points. The resampled map assured an accuracy of ±1.5 m

The measured Hydraulic head map, represented by 31 points, was utilized as observation points (Fig. 5). Pilot points together with a regularization approach were applied to estimate the final conductivity of Rupelian Clay layer during each iteration step.

Pilot points

PEST uses pilot points to bridge the gap between estimating a parameter value in every cell of a model and subdivides models into a small number of homogeneous zones (Doherty 2002). The goal of defining these pilot points is to provide an intermediate approach for characterizing heterogeneity in groundwater models between direct representation of cell-by-cell variability and a reduction in parametrization to a few homogeneous zones (zonation). The pilot point approach assigns a geostatic distribution of parameter values to particular locations. In this study, the location of pilot points coincides with the location of observation points. Therefore, it allows a smaller-scale hydraulic property variation to be represented that can be specified based on the zonation alone. Thus, the modeler is relieved of the responsibility of designing a zonation pattern prior to the model run. An exponential variogram in concert with an ordinary Kriging approach was used for spatial interpolation.

Regularization

Since PEST adjusts the parameter values automatically, the parameters may stay outside a physically acceptable range. Therefore, parameter bounds can be used to limit the adjustment of parameters to a range that is physically acceptable. Adding such constraints to parameters is known as regularization. Two different constraints were set for the lower bound of hydraulic conductivity; scenario *A*, with a lower constraint of 10^{-8} m day^{-1}, and scenario *B*, with a lower constraint of 10^{-16} m day^{-1}. An upper bound

of 10^{-3} m day^{-1} was applied for both scenarios *A* and *B*. The lower limit of 10^{-8} m day^{-1} is a representative value of measured hydraulic conductivity for clay, e.g., Domenico and Schwart (1990), and the lower limit of 10^{-16} m day^{-1} is a representative value of hydraulic conductivity for the Rupelian Clay.

Results

Utilizing the inverse modeling approach, the hydraulic conductivity map of the Rupelian Clay layer was determined. Figure 6 illustrates the objective function versus the number of iterations between FEFLOW and PEST. The optimization simulation of scenario *A* converges after 26 iterations, where the relative phi reduction between iterations $i-1$ and i, $(\Phi_{i-1}-\Phi_i)/\Phi_{i-1}$ is <0.03. The convergence occurred when the calculated hydraulic heads are not sensitive to a change in the hydraulic conductivity (the Jacobian matrix approached zero). This is the case for 0.84 % of the initial objective function, Φ_{init}. The scenario *B* included a wider range of the hydraulic conductivity in the optimization simulation. The minimum of the objective function (Φ) was obtained after seven iterations at 0.86 % of Φ_{init}.

Figure 7a presents the results of the inverse modeling by assuming a lower bound of 10^{-8} m day^{-1} for the Rupelian Clay layer. The hydraulic conductivity map of the Rupelian Clay layer can be divided into three zones: a western zone, a transition zone and a highly conductive zones in the Northeast and Southeast. In general, the hydraulic conductivity increases from west to east. For the western part of Berlin, the hydraulic conductivity is as low as 10^{-8} m day^{-1} . There are two highly conductive zones close to border of Berlin in the Northeast and Southeast. There, the hydraulic conductivity approaches the upper limit of 10^{-3} m day^{-1}. There is a transition zone between the western zone and the highly conductive zones, separated by a low hydraulic conductivity zone in the East, outside of the Berlin border. The hydraulic conductivity in the transition zone ranges between 10^{-4} and 10^{-6} m day^{-1}.

Figure 7b illustrates the hydraulic conductivity map derived by the inverse modeling approach and a lower bound of 10^{-16} m day^{-1}. Both scenarios (*A* and *B*) show some similarities in the distribution of hydraulic conductivity. For example, the hydraulic conductivity approaches the lower limits in the western zone and increases toward

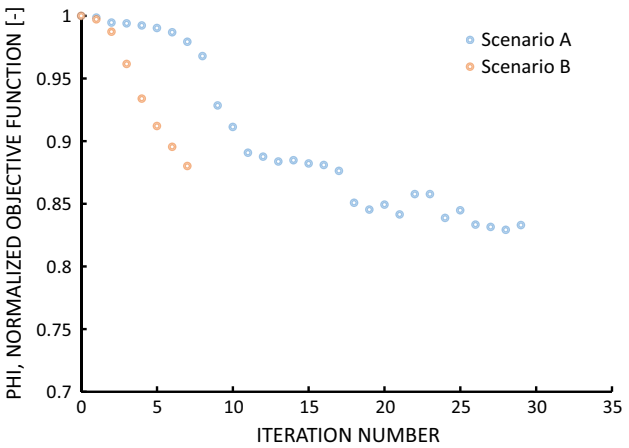

Fig. 6 The normalized objective function as a function of optimization iteration number. The objective function was modified after each iteration and approached a minimum value (see Eq. 10 in "Appendix 3"). Two different scenarios, corresponding to two lower bounds of hydraulic conductivity for the Rupelian Clay, were compared. Scenario *A*: a lower bound of 10^{-8} m day^{-1} and an upper bound of 10^{-3} m day^{-1} were applied. Scenario *B*: a lower bound of 10^{-16} m day^{-1} and an upper bound of 10^{-3} m day^{-1} were applied

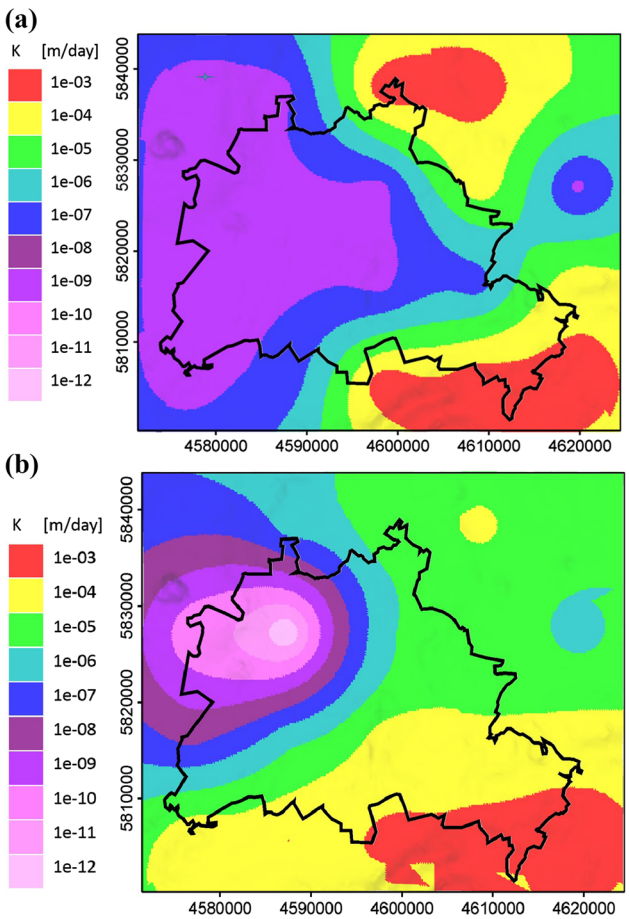

Fig. 7 Spatial distribution of hydraulic conductivity of the Rupelian Clay. Three different zones were recognized: a western zone, a transition zone and highly conductive zones in the Northeast and Southeast of Berlin. **a** Scenario A: hydraulic conductivity of the Rupelian Clay K. **b** Scenario B: hydraulic conductivity of the Rupelian Clay K

the east. In both scenarios, highly conductive zones are present in the Southeast and the Northeast of the Berlin border. The estimated hydraulic conductivities in the Southeast is as high as 10^{-3} m day^{-1} and in the Northeast is as high as 10^{-4} m day^{-1} for both scenarios. The main difference between these two scenarios (regularizations) is the size of the impervious zone, the zone with a hydraulic conductivity lower than 10^{-7} m day^{-1}. This impervious zone is widely distributed in regularization *A*, while it is more restricted to the western region in scenario *B*. Furthermore, scenario *A* presents a larger highly conductive zone in the Northeast of Berlin in comparison with scenario *B*. In contrast, scenario *B* shows a slightly larger highly conductive zone in the Southeast of Berlin.

Figure 8 shows the relation between simulated and observed hydraulic heads for both scenarios. The regression coefficients and standard deviation for both scenarios were compared. Scenario *A* results in a regression coefficient of 0.8062 and standard deviation of 3.69 between simulated and observed data (see Fig. 8a). These values for scenario *B* are a regression coefficient of 0.8015 and a standard deviation of 3.77 (see Fig. 8b).

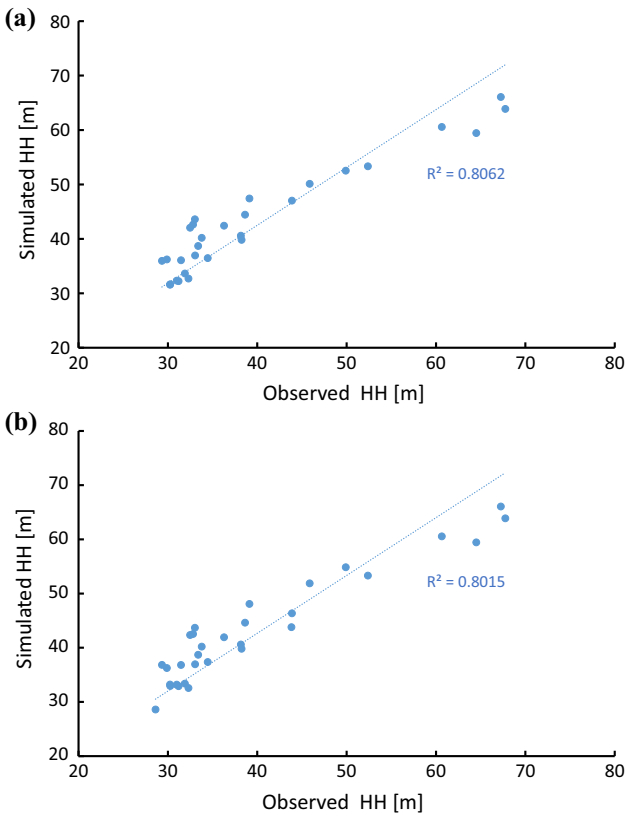

Fig. 8 A comparison between simulated and observed hydraulic heads. **a** Scenario A: simulated hydraulic head versus observed hydraulic head (HH). **b** Scenario B: simulated hydraulic head versus observed hydraulic head (HH)

Having the hydraulic conductivity field of the Rupelian Clay modified, consequences are expected for the coupled fluid flow and heat transport. Therefore, the temperature field for the modified distribution of the hydraulic conductivity was calculated and compared with the initial model.

Forward simulation: the effect of aquitard hydraulic conductivity distribution on the temperature field

Using the updated hydraulic conductivity of the Rupelian Clay as input parameter in an improved forward simulation, the temperature field was investigated by performing a transient simulation for 10^8 days of computational time. The final results were compared with the results of the initial model. The same hydraulic head boundary condition as in the initial model was applied to distinguish the effect of the aquitard hydraulic conductivity distribution on the temperature field. Both derived hydraulic conductivity maps of scenario *A* and scenario *B* were employed to predict the temperature fields. Table 1 summarizes temperature values for both scenarios at different depths below sea level. Table 1 shows that minimum, maximum and mean value of temperatures are quite similar below 2000 m for both scenarios. In contrast to scenario *A*, scenario *B* presents a slightly colder thermal field above 2000 m.

A lower bound of hydraulic conductivity of 10^{-8} m day^{-1} in scenario *A* is more close to the laboratory measured values for Clay. Moreover, scenario *A* better approximates the distribution of the Rupelian Clay layer that is provided by newly available data (see "Model validation" section). Therefore, scenario *A* was chosen to be the base case. Figure 9 shows the predicted temperature values at the top of the Rupelian Clay for scenario *A*. The temperatures are higher in the Northwest and at the southern border of Berlin, where the Rupelian Clay is buried to more than 200 m depth (see Fig. 4).

Table 1 A comparison between predicted temperature fields by scenario *A* and scenario *B*

Depth (m*)	Temperature (°C)					
	Scenario *A*			Scenario *B*		
	Min	Max	Mean	Min	Max	Mean
100	10.4	16.8	13.5	10.1	16.8	13.5
500	15.7	34.2	25.8	12.4	34.2	25.6
1000	29.7	50.0	42.3	24.9	49.6	42.1
2000	65.8	85.7	77.7	65.6	85.5	77.5
3000	90.8	110.2	102.5	88.5	109.9	102.4
4000	115.1	140.5	130.2	115.0	140.3	130.0
5000	152.2	177.5	167.4	152.1	177.5	167.6

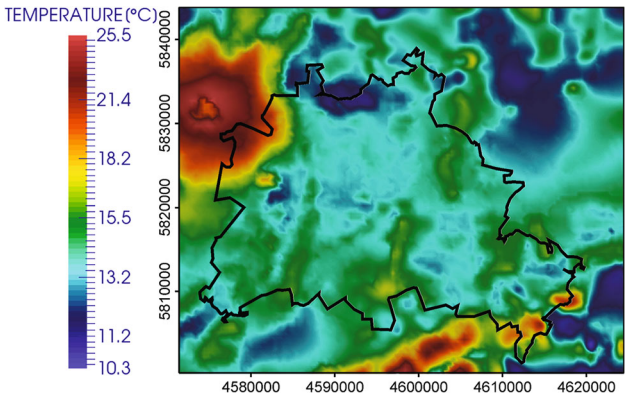

Fig. 9 The predicted temperature field at top of the Rupelian Clay (scenario A)

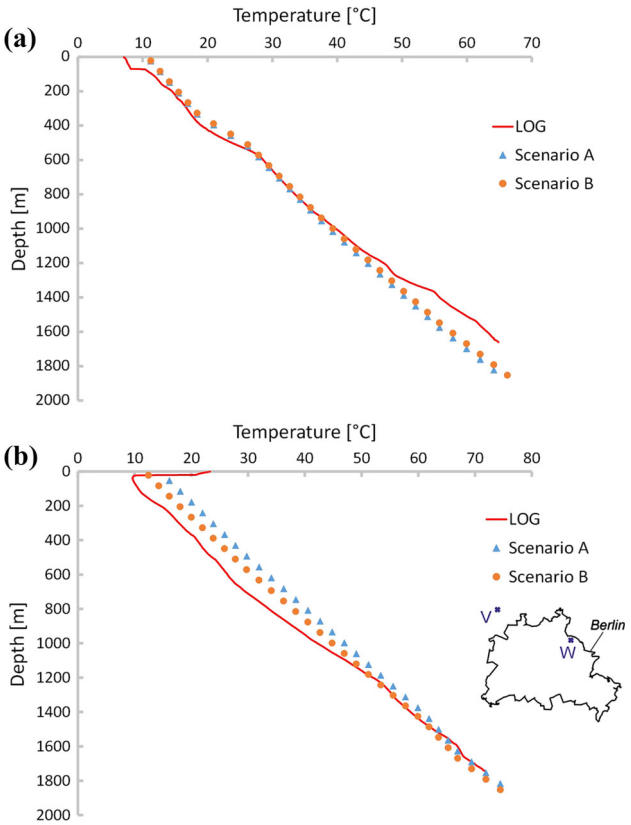

Fig. 10 The model predicted temperatures are compared with measured log temperatures at Velten and Wartenberg boreholes. The predicted temperatures are in the range of borehole-log measurements and follow the same trends. **a** Temperature versus depth. The predicted and measured temperatures at Velten borehole (*V*). **b** Temperature versus depth. The predicted and measured temperatures at Wartenberg borehole (*W*)

Temperature measurements from two wells, Velten and Wartenberg, were used to check the accuracy of the predicted temperatures. Calculated temperatures were plotted versus depth and compared with measured temperatures at existing boreholes (Fig. 10a, b).

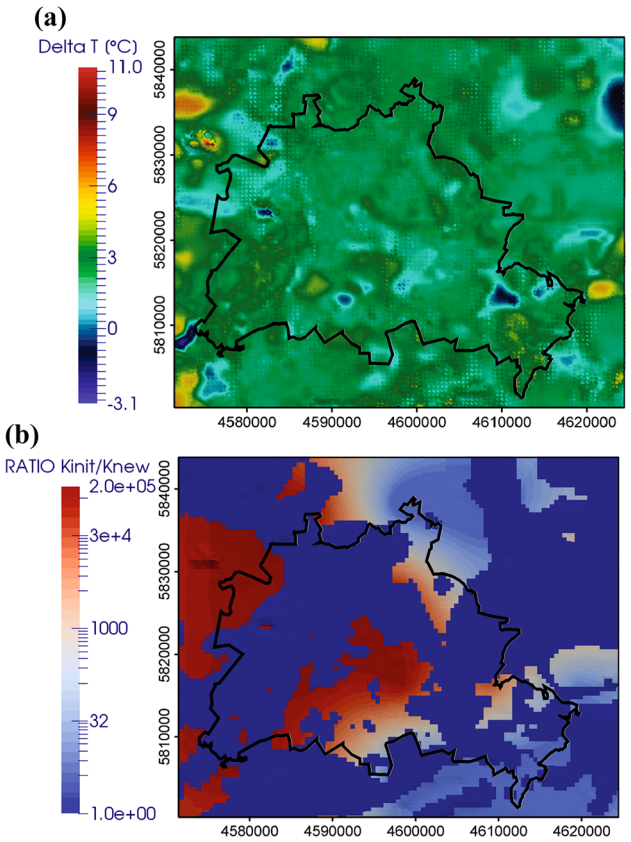

Fig. 11 The temperature field was modified with respect to changes in hydraulic conductivity of the Rupelian Clay (scenario A). The negative temperature difference can be correlated with a strong decrease in conductivity of the Rupelian Clay. **a** Temperature difference between updated and initial temperature field at the top of the Rupelian Clay layer. **b** The ratio between initial and updated (new) hydraulic conductivities at hydrogeological windows (scenario A)

Fig. 12 Difference between temperature fields as calculated by the updated model and by the initial model at different depths (below sea level). Overall, predicted temperature differences are altered due to the changes in hydraulic conductivity of the Rupelian Clay (see Figs. 2b, 7a). The temperature difference is increasing with increasing depth and is more pronounced at deeper levels. **a** 100 m. **b** 500 m. **c** 1000 m. **d** 2000 m. **e** 3000 m. **f** 5000 m. **g** Temperature change, Δ T (°C)

Comparing depth versus temperature plots of calculated and measured temperatures (Fig. 10a, b) reveals that calculated temperatures at Velten borehole match the measurements very well. Here, the modeled temperature is up to 4 °C warmer than the measured temperature below 1400 m. The measured temperatures at the Wartenberg borehole are colder than calculated temperatures at shallow depths and match the calculated temperature below 1200 m.

Figure 11a shows the temperature differences between the initial and updated model (scenario *A*) for the top of the

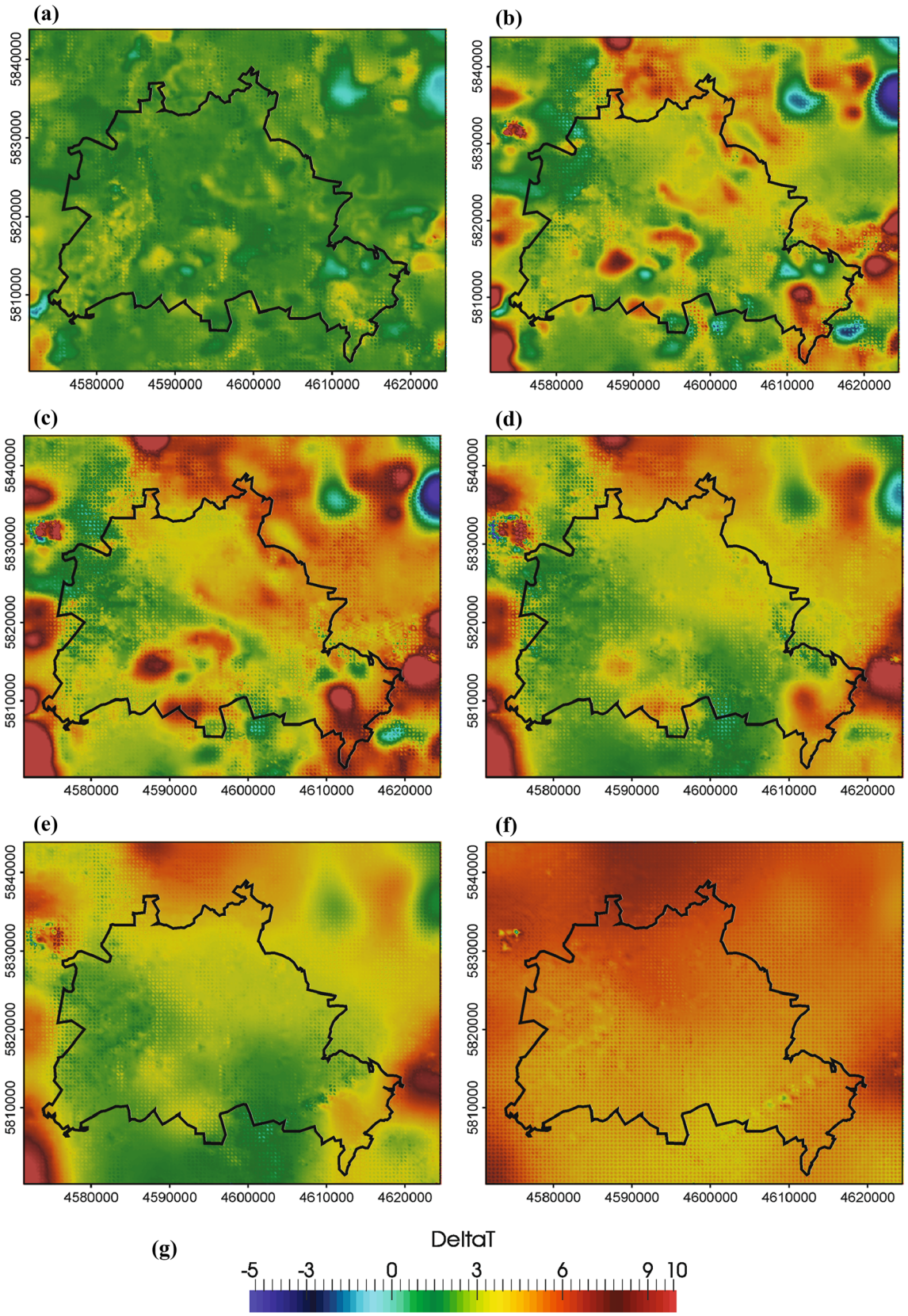
(a)
(b)
(c)
(d)
(e)
(f)
(g)
5840000
5830000
5820000
5810000
4580000
4590000
4600000
4610000
4620000
DeltaT
-5
-3
0
3
6
9
10

Rupelian Clay layer. The temperature difference inversely correlates with changes in hydraulic conductivity (see Fig. 11b). Figure 12 shows the difference between the temperature fields as calculated by the updated model and the initial model at different depths of 100, 500, 1000 2000, 3000, and 5000 m.

It can be observed based on the modeling results that spatially varying interaction between shallow and deep aquifers, as controlled by variations in hydraulic conductivity of the aquitard (Rupelian Clay), influences the temperature field and delimits the depth influence of cold surface water. To quantify the reduced cooling effect of the shallow groundwater entering deeper aquifers, the predicted temperature field of the updated and initial models (see "Initial model: hydrogeological system of Berlin" section) was compared. Figure 12 shows the temperature difference between two models for different depths and illustrates that the overall temperature difference increases with increasing depth. The standard deviation of temperature difference increases to 2.8 °C down to 1000 m (depth measurements refers to the depth below sea level hereafter). Below 1000 m, the standard deviation decreases again to 0.94 °C at 5000 m.

The temperature difference map at 100 m depth cuts the modeled aquifers 1 and 2 that mostly consist of Quaternary unconsolidated sandstones. Here, the temperature predicted by the updated model is in average 2.1 ± 0.7 °C higher than the one predicted by the initial model. The temperature map at 500 m depth cuts different geological units: the Tertiary Rupelian Clay, the Upper and Lower Cretaceous and the Jurassic. At this depth, temperatures are in average 3.4 ± 2.4 °C higher than in the initial model. The largest temperature difference was obtained for the Northeast and Southeast of Berlin area. Temperature distribution becomes more uniform and similar toward the larger depths. The temperature differences vary between 4.2 ± 2.8 °C, 3.6 ± 2.0 °C and 3.4 ± 1.4 °C for 1000, 2000 and 3000 m, respectively. At 5000 m depth, the temperature differences are 5.1 ±0.94 °C.

Discussion

In this study, we applied an inverse modeling approach to characterize the hydraulic conductivity of the Rupelian Clay layer and the location of hydrogeological windows. Then, a forward modeling was employed to characterize the thermal field modifications due to change in hydraulic conductivity of the Rupelian Clay aquitard. The current study includes a more realistic picture of geology where the parameters are varying spatially and includes hydrogeological windows as high conductive areas. The spatial distribution of the aquitard hydraulic conductivity, as representative of the Rupelian Clay distribution, was determined.

Assumptions and limitations

The model presented included inverse modeling and some initial assumptions that were applied in coupling FEFLOW and PEST. The initial model employed a thickness-based distribution of the Rupelian Clay without capturing the water table to characterize the hydrogeological windows, while the inverse modeling included the local hydraulic head data in determining the spatial distribution of hydraulic conductivity of the Rupelian Clay. A constant water table and steady-state flow were assumed, which is justified in the geological time scale; however, the nonlinear interaction between hydraulic conductivity of adjacent layers results in the perturbation in the pressure field (Saltelli et al. 2008; Wainwright et al. 2014) where an unsteady-state condition is required to be employed. Performing inverse modeling simulations under unsteady-state conditions is quite time-consuming, particularly for such a large model. It was also assumed that the physical and hydraulic properties are homogeneous and constant within each of the geological layers except within the Rupelian Clay layer. There are some limited geophysical data available within Berlin area, albeit the vertical resolution of the seismic data sets stays above the minimum thickness of the Rupelian Clay layer, especially in the vicinity of hydrogeological windows that makes seismic data an improper tool in detecting hydrogeological windows. The current approach does not allow to change the geological structure of the model while changing the material properties. A more realistic approach might be updating the geological structure and thickness maps in concert with material properties. Moreover, the subsurface temperatures maps, measured or interpolated data, can also be used in future studies to constrain the thermal conductivity of the aquifers and aquitards to reduce the uncertainty involved.

Model validation

The updated hydraulic conductivity map of the Rupelian Clay (Fig. 7a) suggests an alternative placement and distribution of the Rupelian Clay, and of the hydrogeological windows included. This mean that the hydrogeological windows are present only outside of the city borders, and no interaction between shallow and deep aquifers is expected below the Berlin area. The modified hydrogeological windows are located in the Northeast and Southeast of Berlin. This is in agreement with a recently published model of Tertiary and Quaternary sediments in the Berlin area (Limberg et al. 2014) and the more recent map of the Rupelian Clay thickness [see Fig. 13, courtesy of Frick et al. (2015)].

Not all the potentially small-scale hydrogeological windows were captured because of the uncertainty

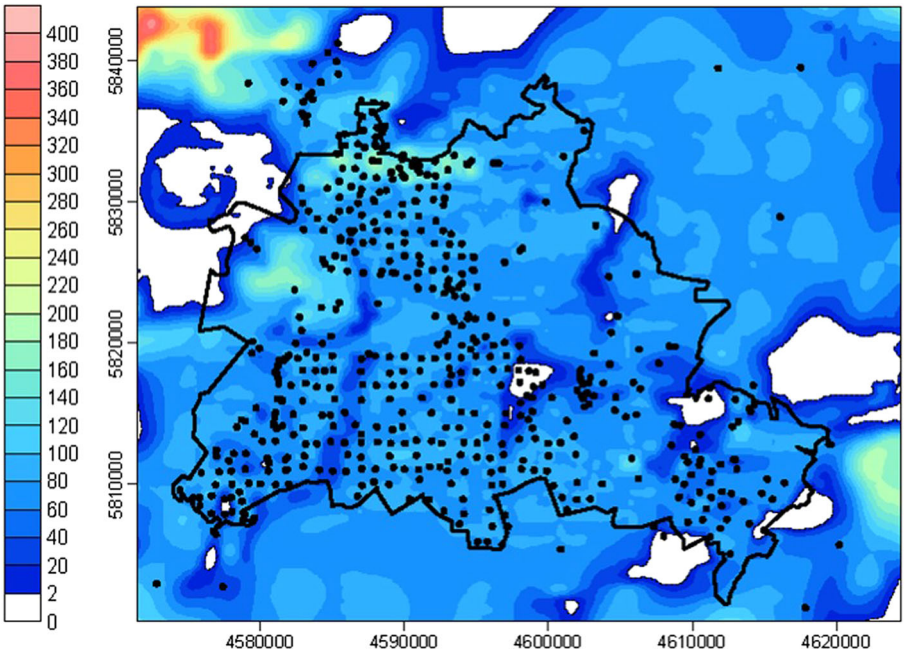

Fig. 13 A recent thickness map of the Rupelian Clay based on new available data. The *circles* represent boreholes reaching the Rupelian Clay (Frick et al. 2015)

involved in available data and the resolution of the inverse modeling approach.

Thermal field and heat transfer mechanisms

The thermal field varies significantly laterally and vertically in the subsurface of Berlin. Thereby, the main controlling features are found to be the complex structure of the geological units and accordingly the spatial distribution of the hydraulic and thermal properties, in response to the geometry of the Zechstein salt layer, and the geometry of the impervious Rupelian Clay layer.

The current study predicts that the Rupelian Clay aquitard is widely distributed and has a quite low hydraulic conductivity. This has two major consequences: First, the hydrogeological windows are restricted and the Rupelian Clay lowers heat conduction to the surface due to its low thermal conductivity, and secondly, convective heat transfer and interaction between shallow and deep aquifers are limited. Therefore, the current model predicts a higher temperature in particular for deeper salty groundwater aquifers (see Fig. 12).

Frick et al. (2015) investigated the thermal field of Berlin area by assuming different heat transfer mechanisms and performed a sensitivity analysis on the hydraulic conductivity of the Rupelian Clay. They concluded that the depth influence of cold surface water is more pronounced when the hydraulic conductivity of the Rupelian Clay is higher. The same behavior can be observed, having a different distribution of hydraulic conductivity for the Rupelian Clay (scenarios *A* and *B*). The size and distribution of the impervious zone within the Rupelian Clay [the zone with hydraulic conductivity lower than 10^{-7} m day^{-1}] influence the temperature field (Table 1). The larger the size of the impervious zone, the lower the groundwater flow-induced cooling effect. This can be observed particularly by comparing the temperature profiles at the Wartenberg well and the warmer temperature profile predicted by scenario *A* in comparison with scenario *B* (Fig. 10b). The temperature profiles are quite similar at the Velten well for both scenarios *A* and *B*, since the Rupelian Clay is impervious there, and the interaction between aquifers is limited (see Fig. 10a). In summary, the advective heat transport mechanism is the dominant heat transport mechanism within the aquifers and hydrogeological windows, whereas the conductive heat transport prevails within the aquitards.

The temperature predicted by the updated model at shallow depth (100 m) is in average 2.1 ± 0.7 °C higher than the one predicted by the initial model. However, this temperature difference is smaller than temperature differences at larger depths. This relatively small change in temperature can be discussed in terms of heat transfer mechanisms, conduction and advection. The model above 100 m is mostly filled with Quaternary and Tertiary deposits with a high thermal conductivity of

4.8 W m^{-1} K^{-1} ("Appendix 1: Table 2") that is equal for initial and updated model. Therefore, the amount of conduction heat transfer is expected to be identical for both initial and updated models in this shallow depth. However, the larger impervious zone at the updated model retards the current of cold surface water downwards. Consequently, the shallow aquifer above the updated Rupelian Clay stays warmer than in the initial model.

At larger depth, the cooling effect of surface water decreases due to the reduced hydraulic conductivity in the domains where hydrogeological windows existed in the initial model. Consequently, less cold surface water penetrates to deeper groundwater aquifers, leading to also warmer temperature at large depths, where the values of porosity and hydraulic conductivity are decreased.

The standard deviation of the temperature difference is zero at the top surface of the model (constant temperature). It increases to 2.8 °C with increasing depth to 1000 m, decreases at larger depths, and is zero again at the base of the model in response to the imposed boundary condition. Accordingly, the standard deviation of the temperature difference is governed by the distance to the thermal model boundaries, by the degree of modification of the hydraulic conductivity, and by heat transfer processes active within the respective depth range.

Applications of the updated map of the Rupelian Clay hydraulic conductivity

The updated map of the Rupelian Clay hydraulic conductivity can be used to determine the degree of hydraulic decoupling between shallow and deep aquifers. That is, decoupling is more pronounced in the West of Berlin where the hydraulic conductivity of the Rupelian Clay aquitard is lower. This decoupling is of major importance for groundwater supply as the freshwater should be protected with respect to contamination by deep saline brine.

A second aspect of this hydraulic decoupling is related to deep penetration of the cold surface water. This aspect results in higher temperatures below areas where the Rupelian Clay layer conductivity is low and consequently is more prospective for geothermal energy exploration.

Conclusion

An inversion approach was successfully examined to characterize a preexisting geological model. The inversion approach estimated the spatial distribution of hydraulic conductivity of a specific aquitard controlling the depth influence of fresh surface water by minimizing the weighted sum of the squared difference between calculated and observed hydraulic heads. Using this approach makes it possible not only to constrain the aquitard hydraulic conductivity but also to detect lateral variations of this parameter in geological models.

For the case study addressed, the results of the inverse modeling suggest a more continuous distribution of the aquitard formation in comparison with earlier model. As this layer separates shallow and deep aquifers, its distribution is the key for the potential penetration of cold shallow water to deeper aquifers.

The spatial variation of the hydraulic conductivity of the Rupelian Clay layer suggests areal lithological and compositional heterogeneities within the Rupelian Clay. In addition, the updated map of the Rupelian Clay hydraulic conductivity indicates that the Rupelian Clay is a continuous layer below the largest part of Berlin and separates shallow freshwater and deep saline aquifers and that the hydrogeological windows are smaller than assumed in earlier models.

Consequently, the convective and advective heat and mass transfer between shallow and deep aquifers below Berlin is most likely limited. The temperature change resulting from the continuity of the Rupelian aquitard results in higher temperatures at depths relevant for deep geothermal exploration below the Rupelian Clay.

Potential future studies should continuously update the structural model of the subsurface of Berlin and aim for further validation of the model based on the temperature and pressure data, to assess the uncertainties involved.

Appendix 1: Properties

Table 2 The average rock thermal and hydraulic properties as input parameter to the model

Geological units	Radiogenic heat prd. ($W\ m^{-1}\ K^{-1}$)	Rock heat cap. ($kJ\ kg^{-1}\ K^{-1}$)	Solid thermal conductivity ($W\ m^{-1}\ K^{-1}$)	Porosity (–)	Hydraulic cond. ($m\ day^{-1}$)
Quaternary 1	0.9	2.16	4.8	0.311	0.001
Tertiary 1	0.9	2.16	4.8	0.311	0.001
Tertiary 2	0.9	2.16	4.8	0.311	0.001
Tertiary 3	1.0	2.16	4.8	0.311	0.001
Rupelian Clay	1.3	2.36	2.2	0.194	0.0001
Pre-Rupelian Clay	1.3	2.26	3.9	0.255	0.001
Upper Cretaceous	0.6	2.29	3.1	0.11	0.05
Lower Cretaceous	1.5	2.29	2.6	0.11	0.05
Jurassic	1.5	2.25	3.2	0.189	0.05
Keuper	1.6	2.32	2.6	0.128	0.01
Muschelkalk	1.0	2.25	2.4	0.036	0.0000001
Upper Buntsandstein	1.8	2.19	3.1	0.025	6.7×10^{-4}
Middle Buntsandstein	1.8	2.39	2.2	0.134	0.06
Lower Buntsandstein	1.8	2.39	1.9	0.049	6.7×10^{-4}
Zechstein	0.4	1.94	4.5	0.005	0.0001
Rotliegend sandstone	1.4	2.18	3.2	0.078	5.26×10^{-3}
Volcanics	2.9	2.6	2.5	0.031	0.00009
Base	2.8	2.3	2.2	0.01	0.0000001

The upper aquifers and aquitard in NGB mainly consist of clay and sandstone. The hydraulic conductivity of clay ranges from 10^{-8} to 10^{-3} $m\ day^{-1}$ and the hydraulic conductivity of sandstone ranges from 10^{-5} to 1 $m\ day^{-1}$. The value of water thermal conductivity is 0.65 $W\ m^{-1}K^{-1}$

Appendix 2: FEFLOW

FEFLOW^{TM} is a finite element-based software package for modeling fluid flow, solute transport and/or heat transport processes in the subsurface (Diersch 2014). The governing equations for unsaturated–saturated flow and heat transport are derived from macroscopic conservation principles for mass, linear momentum and energy.

$$S_0 \frac{\partial h}{\partial t} - \nabla . q = Q \tag{1}$$

$$q = -K \frac{\mu_0^f}{\mu^f} \left(\nabla h + \frac{\rho^f - \rho_0^f}{\rho_0^f} \hat{g} \right) \tag{2}$$

$$\left(S^f(\psi)\epsilon\rho^f c^f + (1-\epsilon)\rho^s c^s\right)\frac{\partial T}{\partial t} + \rho^f c^f q.\nabla T - \nabla.\left[(\Lambda^f + (1-\epsilon)\Lambda^s I)\nabla T\right] + \rho^f c^f Q_h (T - T_0) = Q_T(\psi) \tag{3}$$

All parameters and their units are given in List of Notations. The formulation for steady-state condition can be derived by assuming that partial derivatives with respect to time are zero.

The modeling approach is based on a residual flow method described by Desai and Li (1983). The fixed grid technique mimics the unsaturated flow condition. That is, the physical unsaturated flow is avoided. The element is assumed to be saturated if all its nodes have positive pressure head values ($\psi > 0$). It would be assumed partially saturated if pressure head changes its sign between upper and lower nodes at one element. The element is fully unsaturated if pressure head at all nodes is negative ($\psi < 0$). The pseudo-saturation for each element is a piecewise function of pressure head:

$$S^e = \begin{cases} 1 + \dfrac{(1 - S_r^e)\psi}{h^e}, & \text{if } -h^e < \psi < 0 \\ 1, & \text{if } \psi \geq 0 \\ S_r^e, & \text{if } \psi \leq -h^e \end{cases}$$

A fixed mesh strategy was employed to calculate the vertical location of the free surface (Desai and Li 1983). The depth position of the free surface was computed from the pressure head $p = h - z$. The fixed mesh approach approximates the solution by assuming a linear relation between hydraulic conductivity and storage coefficient (0.0001 [1/m]) as a function of pressure head between saturated and unsaturated zone.

Appendix 3: PEST (Parameter ESTimation)

The parameter estimation attempts to adjust unknown model parameters, such that observations are reproduced utilizing an inverse modeling approach, a mathematical method for determining optimal values of model parameters. In forward modeling, a set of model parameters, initial and boundary conditions are defined to predict the hydraulic head and temperature field. In contrast, the inverse approach uses observed fields (e.g., measured hydraulic head h) to constrain model parameters (e.g., hydraulic conductivity K).

First, the Jacobian matrix is calculated. The elements of the Jacobian matrix are partial differences of observations with respect to the parameters. The partial derivative for each pair of parameters can be calculated by a finite difference approximation. Second, a parameter upgrade vector b is calculated to estimate the next improvements toward the minimum objective function, where it determines the magnitude (step length) and direction toward the minimum objective function.

Assuming a system of equations that includes an input matrix, X as a $m * n$ matrix of known measurements, with m rows and n columns, β as a vector of order n (unknown parameters) and an observation vector y of order m, the matrix system of equations can be written as:

$$X\beta = y \tag{4}$$

The measurements matrix X could include different sets of known parameters, such as layer boundaries, position of electrical signal recorders, inflow across model boundaries, borehole pressure or hydraulic heads. The unknown parameters could be permeability or hydraulic conductivity.

The linear model with several input parameters and variables is given by the following equation:

$$x_{p1}\beta_1 + x_{p2}\beta_2 + \cdots + x_{pn}\beta_n = y_p \tag{5}$$

If the system of equations is linear, the inverse problem can be solved using linear algebra either by using an inversed method ($\beta = X^{-1}y$) or by employing iterative methods, where the residual vector e would be minimized.

$$e = y - X\beta \tag{6}$$

In a nonlinear system, PEST minimizes the sum of squares of residuals $\Phi = \Sigma e_i^2$, to approximate the best vector of variables b. That is, the optimum parameter set, b, can be defined as that for which the sum of squared deviations between model-generated observations and experimental observations is reduced to a minimum.

$$\Phi = \Sigma e_i^2 = e^t e = \|y - Xb\|^2 = (y - Xb)^T (y - Xb) \tag{7}$$

where Φ is the cost function or the least-square estimator, $\|\cdot\|$ is the Euclidean norm, and superscript T stands for transpose matrix. Xb is an approximation of y, and the smaller the difference between observation vector y and Xb the better the approximation.

Furthermore, PEST uses a nonlinear estimation technique known as the Gauss–Marquardt–Levenberg algorithm (GMLA) to optimize the magnitude (step length) and the direction of upgrade of vector b toward minimum. This technique combines two different methods to converge faster toward the minimum objective function: the method of gradient descent and the Gauss–Newton method. The gradient descent takes steps, δb, proportional to the negative of Jacobian matrix, $J(b) = \nabla\Phi(b)$ or the first derivative of the objective function at the current point, to generate a new estimate of b. The Newton method is using a second-order Taylor expansion series to estimate b and requires that the Hessian matrix $H(b)$, second derivative of the objective function, is calculated.

$$\Phi(b + \delta b) = \Phi(b) + J^T \delta b + \frac{1}{2}\delta b H \delta b \tag{8}$$

However, the second derivative of objective function is challenging to compute; thus, a modified approach (Gauss–Newton method) approximates the second derivative by the Jacobian product (Jacobian matrix, J, times its transpose, J^T).

$$\Phi(b + \delta b) = \Phi(b) + J^T \delta b + \delta b J^T J \delta b \tag{9}$$

The GMLA interpolates between the Gauss–Newton algorithm and the method of gradient descent by a scaling parameter, λ. λ has higher values usually at the beginning of minimization, indicating that gradient descent is dominant and step lengths toward the minimum of the objective function are larger. As long as the objective function approaches its minimum, the value of λ decreases and the step lengths shorten. The advantage of this method in comparison with other methods is that it requires a smaller number of runs.

In order to give preference to a particular solution with desirable properties, the regularization objective function, ϕ_r, is included in the minimization of the global objective function Φ, with some suitably chosen multiplier ω:

$$\Phi = \phi_m + \omega\phi_r \tag{10}$$

References

Cardiff M, Barrash W, Kitanidis PK (2013) Hydraulic conductivity imaging from 3-d transient hydraulic tomography at several

pumping/observation densities. Water Resourc Res 49(11):7311–7326
Carrera J, Neuman SP (1986) Estimation of aquifer parameters under transient and steady state conditions: 1. Maximum likelihood method incorporating prior information. Water Resourc Res 22(2):199–210
Desai C, Li G (1983) A residual flow procedure and application for free surface flow in porous media. Adv Water Resour 6:27–35
Diersch HJ (2014) FEFLOW-finite element modeling of flow mass and heat transport in porous and fractured media. Springer, Berlin
Doherty J (2002) Model-independent parameter estimation. In: Watermark numerical computing
Domenico P, Schwart F (1990) Physical and chemical hydrogeology. Wiley, New York
Frick M, Sippel J, Scheck-Wenderoth M, Cacace M, Hassanzadegan A (2015) Influence of shallow flow on the deep geothermal field of Berlin—results from 3D models. In: Geophysical research abstracts, vol 17, EGU2015-5781
Goderniaux P, Davy P, Bresciani E, Dreuz JR, Borgne T (2013) Partitioning a regional groundwater flow system into shallow local and deep regional flow compartments. Water Resourc Res 49(4):2274–2286
Hill MC, Osterby O (2003) Determining extreme parameter correlation in ground water models. Ground Water 41(4):420–430
Jaroch A (2006) Stratifizierung des hydrogeologischen 3d modells von berlin unter berucksichtigung qualifizierter bohrungsinformationen. unpublished master thesis. Master's thesis. Technical University of Berlin
Kaiser BO, Cacace M, Scheck-Wenderoth M, Lewerenz B (2011) Characterization of main heat transport processes in the Northeast German Basin: constraints from 3D numerical models. Geochem Geophys Geosyst 12(7):1–17
Kitanidis PK (1998) How observations and structure affect the geostatistical solution to the steady-state inverse problem. Ground Water 36(5):754–763
Limberg A, Hoermann U, Schneemann J (2014) Geologisches Landesmodell für das Quartär und Tertiär. Senatsverwaltung für Stadtentwicklung und Umwelt. http://berlin.geo-3d.de/berlin3d/portal/
Magri F, Bayer U, Jahnke C, Clausnitzer V, Diersch HJ, Fuhrman J, MÀűller P, Pekdeger A, Tesmer M, Voigt HJ (2005) Fluid-dynamics driving saline water in the North East German Basin. Int J Earth Sci 94(5):1056–1069
Magri F, Bayer U, Pekdeger A, Otto R, Thomsen C, Maiwald U (2009) Salty groundwater flow in the shallow and deep aquifer systems of the Schleswig Holstein area (North German Basin). Tectonophysics 470(1–2):183–194
Neuman SP (1980) A statistical approach to the inverse problem of aquifer hydrology: 3. Improved solution method and added perspective. Water Resourc Res 16(2):331–346
Neuman SP, Yakowitz S (1979) A statistical approach to the inverse problem of aquifer hydrology: 1. Theory. Water Resourc Res 15(4):845–860
Neuman SP, Fogg GE, Jacobson EA (1980) A statistical approach to the inverse problem of aquifer hydrology: 2. Case study. Water Resourc Res 16(1):33–58
Poeter EP, Hill MC (1997) Inverse models: a necessary next step in ground-water modeling. Ground Water 35(2):250–260
Saltelli A, Ratto M, Andres T, Campolongo F, Cariboni J, Gatelli D, Saisana M, Tarantola S (2008) Global sensitivity analysis: the primer. Wiley, New York
Stackebrandt W (2010) Atlas zur geologie von brandenburg. In: Technical report, Landesamt fAijr Bergbau, Geologie und Rohstoffe Brandenburg
Wainwright HM, Finsterle S, Jung Y, Zhou Q, Birkholzer JT (2014) Making sense of global sensitivity analyses. Comput Geosci 65:84–94 (TOUGH Symposium 2012)
Zhou H, Gomez-Hernandez JJ, Li L (2014) Inverse methods in hydrogeology: evolution and recent trends. Adv Water Resourc 63:22–37